

A Scaling Law for the Orbital Architecture of Planetary Systems Formed by Gravitational Scattering and Collisions

EIICHIRO KOKUBO,^{1,2,3} HARUKA HOSHINO,^{3,1} YUJI MATSUMOTO,² AND RE'EM SARI⁴

¹*Division of Science, National Astronomical Observatory of Japan, Osawa, Mitaka, Tokyo 181-8588, Japan*

²*Center for Computational Astrophysics, National Astronomical Observatory of Japan, Osawa, Mitaka, Tokyo 181-8588, Japan*

³*Department of Astronomy, University of Tokyo, Hongo, Bunkyo, Tokyo 113-0033, Japan*

⁴*Racah Institute of Physics, Hebrew University of Jerusalem, 9190401, Israel*

ABSTRACT

In the standard formation models of terrestrial planets in the solar system and close-in super-Earths in non-resonant orbits recently discovered by exoplanet observations, planets are formed by giant impacts of protoplanets or planetary embryos after the dispersal of protoplanetary disk gas in the final stage. This study aims to theoretically clarify a fundamental scaling law for the orbital architecture of planetary systems formed by giant impacts. In the giant impact stage, protoplanets gravitationally scatter and collide with one another to form planets. Using N -body simulations, we investigate the orbital architecture of planetary systems formed from protoplanet systems by giant impacts. As the orbital architecture parameters, we focus on the mean orbital separation between two adjacent planets and the mean orbital eccentricity of planets in a planetary system. We find that the orbital architecture is determined by the ratio of the two-body surface escape velocity of planets v_{esc} to the Keplerian circular velocity v_K , $k = v_{\text{esc}}/v_K$. The mean orbital separation and eccentricity are about $2ka$ and $0.3k$, respectively, where a is the system semimajor axis. With this scaling, the orbital architecture parameters of planetary systems are nearly independent of their total mass and semimajor axis.

1. INTRODUCTION

Current exoplanet surveys reveal that many planets in the Galaxy are close-in planets with semimajor axes smaller than about 0.3 au and masses smaller than about 30 Earth masses (e.g., [Mayor et al. 2011](#); [Howard et al. 2012](#); [Petigura et al. 2017](#)). Their composition is not yet well constrained, but most may consist mainly of solid components. In the present paper, we call these planets close-in super-Earths. For general characteristics of the planets, refer to [Weiss et al. \(2023\)](#). Many of these exoplanets reside in multiplanet systems (e.g., [Batalha et al. 2013](#)), and some studies estimate that the typical multiplicity of close-in super-Earths is around three (e.g., [Zhu et al. 2018](#)). The distribution of period ratios between pairs of adjacent planets roughly follows a log-normal distribution with slight excess around some low-order mean motion resonances (e.g., [Baruteau & Papaloizou 2013](#); [Winn & Fabrycky 2015](#)). The orbital separation between adjacent pairs is in the range of 10-40 r_H with a peak around 20 r_H , where r_H is the mutual Hill radius, which is smaller than the mean value of the solar system terrestrial planets, 43 r_H (e.g., [Lissauer et al. 2014](#); [Weiss et al. 2018](#)). While the orbits of single planets tend to be more eccentric, those of planets in multiplanet systems

tend to have smaller eccentricities and inclinations of a few percent (e.g., Xie et al. 2016; Hadden & Lithwick 2017; He et al. 2020). In other words, the close-in super-Earth systems are dynamically compact and cold. In addition, most multiplanet systems show an intrasystem uniformity called the “peas-in-a-pod” pattern in which planets have nearly equal radii and regularly spaced, nearly circular, and coplanar orbits (e.g., Weiss et al. 2018; Millholland & Winn 2021; Weiss et al. 2023).

It is widely accepted that the final stage of terrestrial planet formation in the solar system involves giant impacts among protoplanets or planetary embryos (e.g., Kokubo & Ida 2012; Raymond et al. 2014). In this stage, protoplanets gravitationally scatter and collide with one another to form planets, and then the orbital structure is determined. The same is assumed for some formation models of the super-Earth systems, where planets are formed through giant impacts after the dispersal of disk gas from a protoplanet system that are formed in situ or by migration from the outer disk (e.g., Hansen & Murray 2012; Lee & Chiang 2016; Ogiwara et al. 2018; Matsumoto et al. 2020). Although the formation timescale of protoplanets may be shorter than the lifetime of a gas disk, the presence of gas imposes dynamical friction that circularizes their orbits and prevents their mutual collisions. The giant impact phase is then delayed until most of the gas leaves the system. One of this model’s merits is the natural formation of planets in non-resonant orbits. In this paper, we focus on the general dynamics of the giant impact evolution that may be responsible for creating the non-resonant close-in super-Earth systems. We therefore examine an idealized model of giant impacts, starting with nearly circular, slightly inclined orbits without disk gas.

There are many studies on the giant impact formation of terrestrial planets in the solar system and super-Earths (e.g., Chambers & Wetherill 1998; Kokubo et al. 2006; Ogiwara et al. 2018). However, only a few papers focused on the orbital architecture of multiplanet systems, such as the mean orbital separation between adjacent planets and the mean orbital eccentricity of planets in a system. As one of the few examples, Hoshino & Kokubo (2023) investigated the effects of stellar mass on orbital architecture and found that a planetary system becomes dynamically more compact and colder as the stellar mass increases. As a related study, Ghosh & Chatterjee (2024) also examined the effect of dynamical instability on the orbital architecture of multiplanet systems.

This study aims to obtain a general scaling law for the orbital architecture of planetary systems formed by giant impacts. We perform N -body simulations of the giant impact stage from protoplanet systems. We clarify how a protoplanet system evolves through gravitational scattering and collisions among protoplanets and what determines the final system configuration.

We describe the calculation method in Section 2 and present the results in Section 3. Section 4 is devoted to a summary and discussion.

2. CALCULATION METHOD

2.1. Initial Protoplanet Systems

We perform N -body simulations of the giant impact stage from protoplanet systems. We adopt idealized protoplanet systems to facilitate understanding of the elementary process of orbit determination by giant impacts and its dependence on system parameters. For simplicity, we assume that the global mass distribution of protoplanets obeys the solid surface density distribution given by

$$\Sigma = \Sigma_1 \left(\frac{r}{1 \text{ au}} \right)^{-2}, \quad (1)$$

Table 1. Initial Conditions of Protoplanet Systems

model	Σ_1 (gcm $^{-2}$)	r_{in} (au)	r_{out} (au)	σ_e	N	M_{tot} (M_{\oplus})	a_M (au)
S0	10	0.1	0.3	0.01	15	2.44	0.17
M1	5			0.005	22	1.26	0.18
M2	20			0.014	11	5.06	0.18
M3	50			0.022	7	12.75	0.18
R1		0.05	0.15				0.09
R2		0.2	0.6				0.35
R3		0.5	1.5				0.87

NOTE— Blank spaces assume an identical parameter as the standard model S0.

with inner and outer cutoffs, r_{in} and r_{out} , where Σ_1 is the reference surface density at 1 au, and r is the radial distance from the central star. Since the giant impact stage starts after the dispersal of disk gas, we assume a gas-free disk. We systematically vary the disk parameters: $\Sigma_1 = 5, 10, 20, 50 \text{ gcm}^{-2}$, and $(r_{\text{in}}, r_{\text{out}}) = (0.05, 0.15), (0.1, 0.3), (0.2, 0.6), (0.5, 1.5)$ (the unit is au). We set the central star's mass equal to the solar mass $M_* = M_{\odot}$.

The isolation mass gives the protoplanet mass M

$$M_{\text{iso}} \simeq 2\pi ab\Sigma = 0.16 \left(\frac{\Sigma_1}{10} \right)^{3/2} M_{\oplus}, \quad (2)$$

where a is the semimajor axis of a protoplanet, b is the orbital separation between adjacent protoplanets, and M_{\oplus} is the Earth mass, and we assume $b = 10r_{\text{H}}$ (Kokubo & Ida 1998, 2002). The mutual Hill radius for protoplanets j and $j + 1$ is given by

$$r_{\text{H},j} = h_j \frac{a_j + a_{j+1}}{2}, \quad (3)$$

where h_j is given by

$$h_j = \left(\frac{M_j + M_{j+1}}{3M_*} \right)^{1/3}, \quad (4)$$

where protoplanet numbers j are sorted in ascending order by a . Note that the $\Sigma \propto r^{-2}$ disk corresponds to an equal-mass protoplanet system. The initial eccentricities e and inclinations i of protoplanets are given by the Rayleigh distribution with dispersions $\sigma_e = 2\sigma_i = 0.01(\Sigma_1/10)^{1/2}$ (the unit of i is radian). We assume spherical protoplanets with the bulk density $\rho = 3 \text{ gcm}^{-3}$. The initial conditions of protoplanet systems ($\Sigma_1, r_{\text{in}}, r_{\text{out}}, \sigma_e$) are summarized in Table 1 with their system properties: protoplanet number N , total mass M_{tot} , and mass-weighted mean semimajor axis $a_M = \sum_j^N M_j a_j / \sum_j^N M_j$. We refer to model S0 as the standard model. We perform 20 runs for each model with different initial angular distributions of protoplanets.

2.2. Time Evolution

The orbits of protoplanets are calculated by numerically integrating the equation of motion of protoplanets. For numerical integration, we use the modified Hermite integrator for planetary N -body simulation (Kokubo et al. 1998; Kokubo & Makino 2004) with the hierarchical timestep (Makino 1991). We use the Phantom GRAPE scheme

Table 2. Physical and Orbital Properties of Planetary Systems

model	$\langle N \rangle$	$\langle M_{\max} \rangle (M_{\oplus})$	$\langle M_{\text{ave}} \rangle (M_{\oplus})$	$\langle \sigma_M / M_{\text{ave}} \rangle$	$\langle \tilde{b}_H \rangle$	$\langle \tilde{e}_H \rangle$	$\langle \tilde{i}_H \rangle$	$\langle \tilde{b}_K \rangle$	$\langle \tilde{e}_K \rangle$	$\langle \tilde{i}_K \rangle$	$\langle \sigma_{\tilde{b}_H} / \tilde{b}_H \rangle$
S0	5.0 ± 1.0	0.81 ± 0.16	0.49 ± 0.08	0.38 ± 0.09	24.56 ± 2.46	3.10 ± 0.70	1.87 ± 0.57	2.16 ± 0.20	0.29 ± 0.05	0.16 ± 0.04	0.14 ± 0.06
M1	6.0 ± 1.0	0.29 ± 0.00	0.21 ± 0.03	0.27 ± 0.04	24.78 ± 2.69	3.17 ± 0.60	2.16 ± 0.69	2.26 ± 0.24	0.28 ± 0.06	0.18 ± 0.07	0.13 ± 0.03
M2	4.0 ± 1.0	1.83 ± 0.46	1.26 ± 0.25	0.26 ± 0.10	23.75 ± 3.34	2.77 ± 0.74	2.07 ± 0.90	2.12 ± 0.25	0.25 ± 0.07	0.18 ± 0.08	0.15 ± 0.07
M3	3.0 ± 1.0	5.44 ± 1.80	4.23 ± 1.10	0.38 ± 0.13	20.18 ± 3.94	2.64 ± 0.77	1.37 ± 0.48	1.81 ± 0.29	0.23 ± 0.08	0.12 ± 0.04	0.08 ± 0.05
R1	6.0 ± 0.5	0.65 ± 0.00	0.41 ± 0.03	0.34 ± 0.05	20.92 ± 1.52	2.36 ± 0.45	1.44 ± 0.58	2.66 ± 0.18	0.31 ± 0.07	0.17 ± 0.07	0.16 ± 0.02
R2	3.5 ± 0.5	0.97 ± 0.16	0.71 ± 0.10	0.39 ± 0.15	34.31 ± 2.89	5.54 ± 1.96	3.84 ± 0.95	2.10 ± 0.20	0.35 ± 0.12	0.23 ± 0.04	0.14 ± 0.04
R3	3.0 ± 0.5	1.46 ± 0.16	0.70 ± 0.09	0.77 ± 0.15	54.40 ± 8.91	11.98 ± 3.00	10.36 ± 3.58	1.97 ± 0.29	0.43 ± 0.10	0.36 ± 0.11	0.11 ± 0.10

(Nitadori et al. 2006) to efficiently compute mutual gravity among protoplanets. The simulations follow the evolution of protoplanet systems for at least $5 \times 10^8 t_K$ of the innermost protoplanet, where t_K is the Kepler period.

During orbital integration, when two protoplanets contact, a collision occurs. For simplicity, we adopt perfect accretion as the collision model, where every collision leads to accretion. The dynamical properties of planets formed by giant impacts barely change even if hit-and-run collisions are considered (Kokubo & Genda 2010).

2.3. System Parameters

We investigate the properties of not individual planets but a planetary system as a whole. We introduce the architecture parameters normalized by the mutual Hill radius, which are the mean orbital separation between adjacent planets j and $j + 1$

$$\tilde{b}_H = \frac{1}{N-1} \sum_j^{N-1} \frac{a_{j+1} - a_j}{r_{H,j}}, \quad (5)$$

and the mean eccentricity (epicycle amplitude)

$$\tilde{e}_H = \frac{1}{N-1} \sum_j^{N-1} \frac{a_j e_j + a_{j+1} e_{j+1}}{2r_{H,j}}. \quad (6)$$

We calculate \tilde{i}_H in the same way. Note that with this definition \tilde{e}_H is addable to \tilde{b}_H . To measure the separation uniformity in a system, we calculate the standard deviation $\sigma_{\tilde{b}_H}$ of \tilde{b}_H , and inspect the normalized separation deviation $\sigma_{\tilde{b}_H} / \tilde{b}_H$. As the system semimajor axis, we use the mass-weighted mean semimajor axis of planets a_M . For example, the terrestrial planet system in the solar system has $\tilde{b}_H = 43$, $\tilde{e}_H = 5$, $\sigma_{\tilde{b}_H} / \tilde{b}_H = 0.35$ and $a_M = 0.9$ au.

In addition, as the physical properties of a planetary system, we calculate the number N , maximum mass M_{\max} , average mass M_{ave} , and mass ratio between standard deviation and average $\sigma_M / M_{\text{ave}}$ of planets. Note that the number of planets per unit logarithmic semimajor axis is given by $N / \log(r_{\text{out}} / r_{\text{in}}) = N / \log 3$.

We calculate the median and median absolute deviation of these parameters in 20 runs for each model, which are given with $\langle \cdot \rangle$.

3. RESULTS

We investigate the orbital architecture of planetary systems formed from protoplanet systems by giant impacts. Firstly, we show the time evolution of the orbital architecture from protoplanet systems to planetary systems in

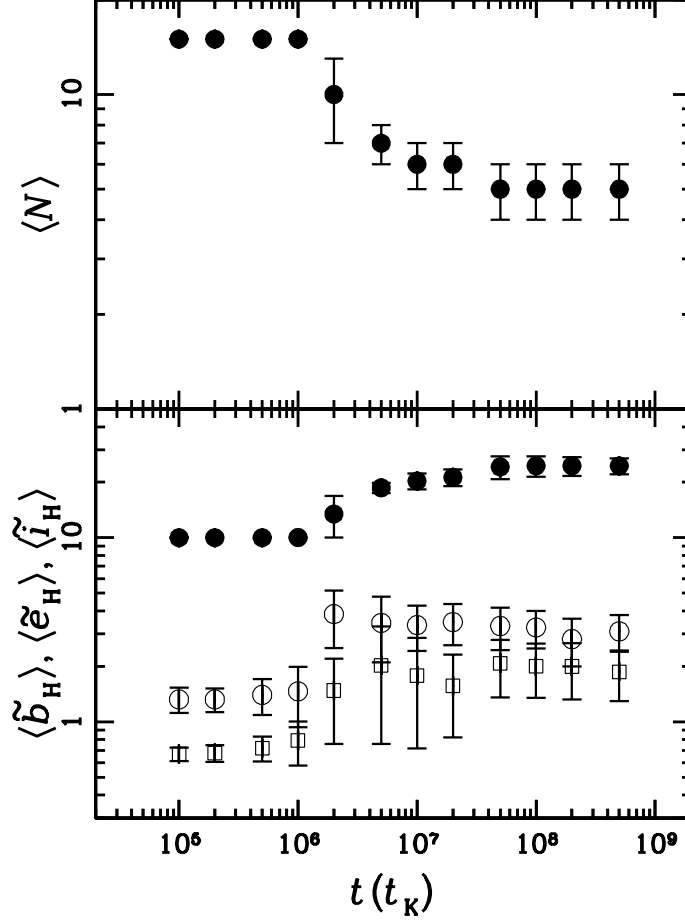


Figure 1. Time evolution of the number $\langle N \rangle$ (top panel) and the normalized orbital separation between adjacent pairs $\langle \tilde{b}_H \rangle$ (filled circles), eccentricity $\langle \tilde{e}_H \rangle$ (open circles), and inclination $\langle \tilde{i}_H \rangle$ (open squares) (bottom panel) of the standard protoplanet systems (model S0). The values and error bars indicate the median and median absolute deviation in 20 runs, respectively.

Section 3.1. We next examine how the orbital architecture depends on the system mass and semimajor axis in Sections 3.2 and 3.3. Then, we derive a scaling law of the orbital architecture in Section 3.4. The statistical results of the physical and orbital properties of all models are summarized in Table 2.

3.1. Time Evolution

Firstly, we show the time evolution of the orbital architecture using the standard model (model S0). The averaged number of planets and scaled orbital architecture calculated from 20 runs are plotted against time in Figure 1. The system is quite stable for about $10^6 t_K$ in the sense that the orbital architecture shows no substantial changes. None of the systems exhibit a merger before $10^6 t_K$, while several mergers typically occur before $2 \times 10^6 t_K$, reducing the number of bodies on average by 1/3. The giant impact stage lasts for several $10^7 t_K$ forming planetary systems, which are stable for longer than $10^8 t_K$. This evolution is seen in the number of planets $\langle N \rangle$ in Figure 1. The initial parameters of the orbital architecture are $\tilde{b}_H = 10$ and $\tilde{e}_H \simeq 2\tilde{i}_H \simeq 1.3$ in this model. We find that when and after the giant impact stage begins, $\langle \tilde{e}_H \rangle$ and $\langle \tilde{i}_H \rangle$ increase rapidly and then become almost constant with time, while $\langle \tilde{b}_H \rangle$ increases monotonically with time. This is the typical evolution of the scaled orbital architecture by giant impacts. The final

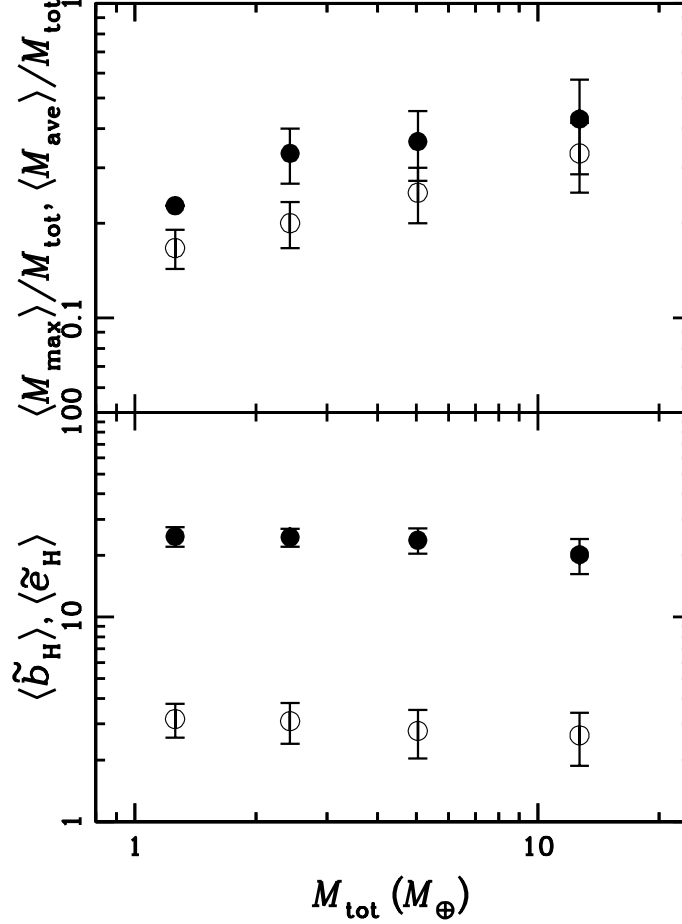


Figure 2. Maximum $\langle M_{\max} \rangle$ (filled circles) and average $\langle M_{\text{ave}} \rangle$ (open circles) masses of planets normalized by the system total mass M_{tot} (top panel) and the normalized orbital separation between adjacent pairs $\langle \tilde{b}_{\text{H}} \rangle$ (filled circles) and eccentricity $\langle \tilde{e}_{\text{H}} \rangle$ (open circles) (bottom panel) against the total mass of protoplanet systems with the reference surface density $\Sigma_1 = 5, 10, 20$, and 50 (models S0 and M1-3).

parameters of the orbital architecture are $\langle \tilde{b}_{\text{H}} \rangle \simeq 25$, $\langle \tilde{e}_{\text{H}} \rangle \simeq 3.1$, and $\langle \tilde{i}_{\text{H}} \rangle \simeq 1.9$, which are determined by the orbital (in)stability.

We find that compared to previous works that investigated giant impact evolution with the larger semimajor axis ($a \sim 1$ au) (e.g., Kokubo et al. 2006), a more compact, dynamically colder planetary system is formed. The origin of this difference by the semimajor axis will be discussed in detail in Section 3.3. As could be expected from giant impacts, the planet’s orbits in the final systems are basically not in mean motion resonances, consistent with most observed Kepler planets (e.g., Winn & Fabrycky 2015). The orbital separation is also consistent with the mode of the orbital separation distribution of Kepler multiplanet systems in the same region (e.g., Lissauer et al. 2014). The ratio between the mean eccentricity and inclination is $\langle \tilde{i}_{\text{H}} \rangle / \langle \tilde{e}_{\text{H}} \rangle \sim 0.5$, which is typical for planetary systems formed by giant impacts (e.g., Kokubo et al. 2006; Matsumoto & Kokubo 2017). Since the inclination’s behavior is similar to the eccentricity in the present parameter range, we focus on the eccentricity hereafter.

We find that the orbital architecture parameters converge to certain values. The next step is to examine how these values depend on the system parameters.

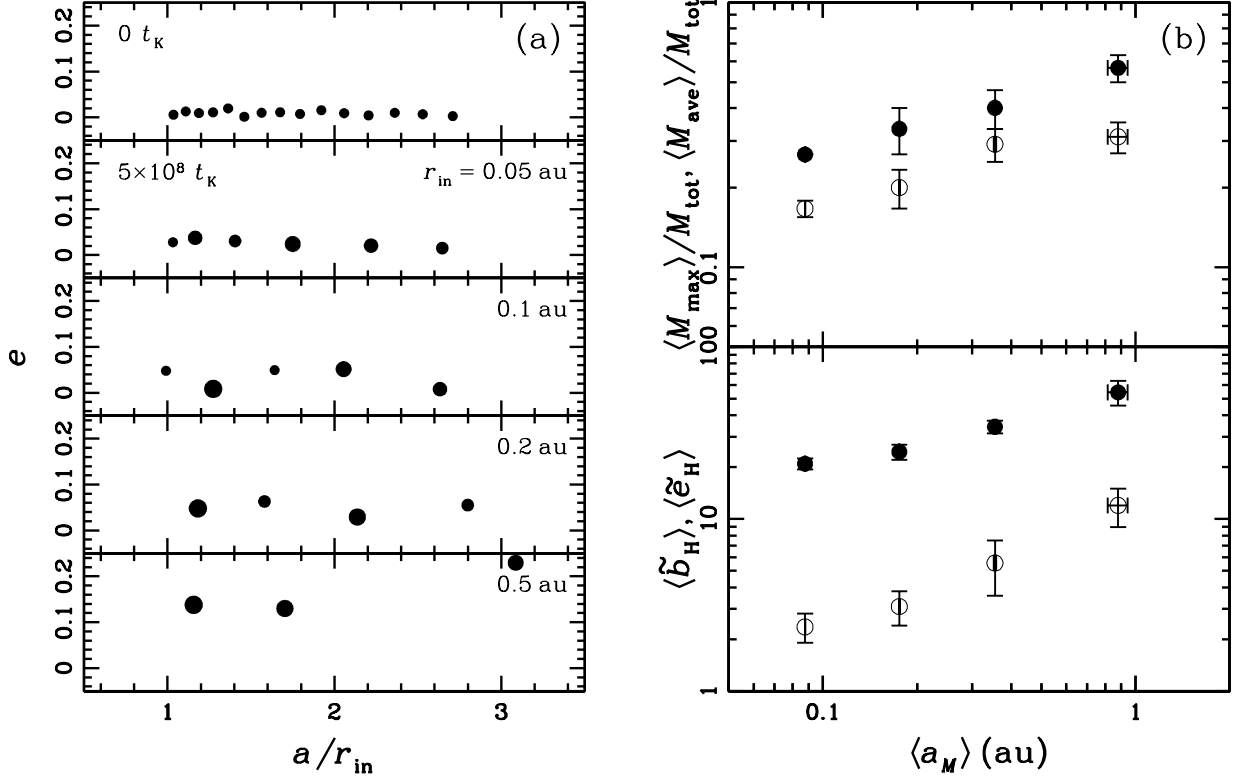


Figure 3. Panel a (left): Examples of the final planetary system on the semimajor-axis a -eccentricity e plane, where a is scaled by the inner edge radius r_{in} for protoplanet systems at different locations (models S0 and R1-3), together with the initial protoplanet system (top panel). The sizes of the circles are proportional to the physical sizes of the planets. Panel b (right): Maximum $\langle M_{\text{max}} \rangle$ (filled circles) and average $\langle M_{\text{ave}} \rangle$ (open circles) masses of planets (top panel) and the orbital separation between adjacent pairs $\langle \tilde{b}_H \rangle$ (filled circles) and eccentricity $\langle \tilde{e}_H \rangle$ (open circles) normalized by the Hill radius r_H (bottom panel) against the system semimajor axis $\langle a_M \rangle$ for $(r_{\text{in}}, r_{\text{out}}) = (0.05, 0.15)$, $(0.1, 0.3)$, $(0.2, 0.6)$, and $(0.5, 1.5)$ (the unit is au) (models S0 and R1-3).

3.2. Dependence on System Mass

We investigate the effects of the disk parameter Σ_1 on the orbital architecture of planetary systems by comparing models with $\Sigma_1 = 5, 10, 20$, and 50 (models S0 and M1-3). Changing Σ_1 corresponds to changing the individual initial and total protoplanet masses. The total mass of protoplanets increases in proportion to Σ_1 . Figure 2 shows the maximum and average masses of planets and the normalized orbital separation and eccentricity of planetary systems against the total protoplanet mass M_{tot} . As evident from the top panel of Figure 2, $\langle M_{\text{max}} \rangle$ and $\langle M_{\text{ave}} \rangle$ increase with M_{tot} (Kokubo et al. 2006). Correspondingly, $\langle N \rangle$ decreases with increasing M_{tot} as in Table 2. By the least-square-fit method, we obtain $d \log(\langle M_{\text{max}} \rangle / M_{\text{tot}}) / d \log M_{\text{tot}} \simeq d \log(\langle M_{\text{ave}} \rangle / M_{\text{tot}}) / d \log M_{\text{tot}} \simeq 0.3$. The normalized mass deviation $\langle \sigma_M / M_{\text{ave}} \rangle$ is about 0.3-0.4, which is consistent with Goldberg & Batygin (2022).

We also find that both \tilde{b}_H and \tilde{e}_H barely depend on M_{tot} with $d \log \langle \tilde{b}_H \rangle / d \log M_{\text{tot}} \simeq d \log \langle \tilde{e}_H \rangle / d \log M_{\text{tot}} \simeq -0.09$. In other words, the orbital parameters of planetary systems with different masses can be scaled by the Hill radius. The orbital separations in a system for all models are relatively uniform with $\sigma_{\tilde{b}_H} / \tilde{b}_H = 0.08$ -0.15.

3.3. Dependence on System Semimajor Axis

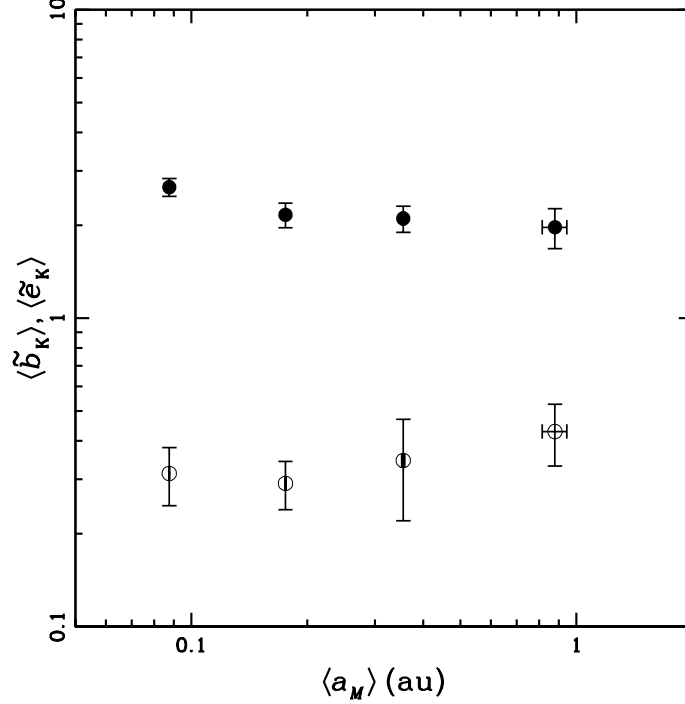


Figure 4. Orbital separation between adjacent pairs $\langle \tilde{b}_K \rangle$ (filled circles) and eccentricity $\langle \tilde{e}_K \rangle$ (open circles) normalized by the eccentric distance r_K against the system semimajor axis $\langle a_M \rangle$ for $(r_{\text{in}}, r_{\text{out}}) = (0.05, 0.15), (0.1, 0.3), (0.2, 0.6),$ and $(0.5, 1.5)$ (the unit is au) (models S0 and R1-3).

Next, we investigate how the orbital architecture of planetary systems depends on the initial location of protoplanet systems (models S0 and R1-3). Note that with $\Sigma \propto r^{-2}$, N and M_{tot} are the same in all these models.

In Figure 3a, the final planetary systems of an example run for each model are shown in the $a/r_{\text{in}}-e$ plane, where the semimajor axis is scaled by r_{in} , and the initial protoplanet systems are the same in this plane. During formation, the mean semimajor axis of the system is kept almost constant. For systems located farther away from the star (larger r_{in}), the number of planets decreases, while the eccentricities and relative orbital separations to the semimajor axis increase.

Figure 3b plots $\langle M_{\text{max}} \rangle$, $\langle M_{\text{ave}} \rangle$, $\langle \tilde{b}_H \rangle$ and $\langle \tilde{e}_H \rangle$ against the system semimajor axis $\langle a_M \rangle$. We find that both $\langle M_{\text{max}} \rangle$ and $\langle M_{\text{ave}} \rangle$ increase with $\langle a_M \rangle$ as well as $\langle \sigma_M / M_{\text{ave}} \rangle$ in Table 2. This $\langle \sigma_M / M_{\text{ave}} \rangle$ dependence indicates that the mass distribution in the inner disk can be more uniform than in the outer disk. The dependencies of $\langle M_{\text{max}} \rangle$ and $\langle M_{\text{ave}} \rangle$ on $\langle a_M \rangle$ are $d \log(\langle M_{\text{max}} \rangle / M_{\text{tot}}) / d \log \langle a_M \rangle \simeq d \log(\langle M_{\text{ave}} \rangle / M_{\text{tot}}) / d \log \langle a_M \rangle \simeq 0.3$. We find that as $\langle a_M \rangle$ decreases, $\langle \tilde{b}_H \rangle$ and $\langle \tilde{e}_H \rangle$ decrease, in other words, the system becomes more compact and dynamically colder in the inner disk. We obtain $d \log \langle \tilde{b}_H \rangle / d \log \langle a_M \rangle \simeq 0.4$ and $d \log \langle \tilde{e}_H \rangle / d \log \langle a_M \rangle \simeq 0.7$. This trend is because in the inner disk, collisions are relatively more effective than gravitational scattering since the Hill radius decreases with the semimajor axis, and thus accretion proceeds in a tournament-chart-like way on the $a-M$ plane (e.g., Matsumoto & Kokubo 2017; Hoshino & Kokubo 2023). The smaller eccentricities realized by collisional damping allow for narrower orbit spacings. Again, the orbital separation deviation is less than or equal to 0.16 as shown in Table 2, which means rather uniformly spaced orbits. Note that the resultant orbital separation 54.40 ± 8.91 for $\langle a_M \rangle = 0.87$ au (model R3) is generally consistent with that of the solar system terrestrial planets, 43.

3.4. New Scaling

The orbital architecture parameters of planetary systems do not depend on the system mass but on the system semimajor axis. Based on these results, let us consider a scaling law for the orbital architecture.

Here, we introduce a new characteristic length scale that renormalizes the relative importance of gravitational scattering and collisions described above. When a planetesimal system evolves under gravitational scattering and collisions, the random velocity of planetesimals becomes as large as their two-body surface escape velocity v_{esc} (e.g., [Safronov 1972](#); [Kokubo & Ida 1996](#)). We adopt this idea, although there are fewer bodies in protoplanet systems than in planetesimal systems. Under this equilibrium, the characteristic eccentricity, often called "escape eccentricity" is given by $k = v_{\text{esc}}/v_K$, where v_K is the Kepler circular velocity. Using k , we introduce the characteristic length scale r_K corresponding to the eccentric distance or the amplitude of the radial excursion (epicycle amplitude). In the same way as the Hill radius, r_K for planets j and $j + 1$ is defined as

$$r_{K,j} = k_j \frac{a_j + a_{j+1}}{2}, \quad (7)$$

where

$$k_j = \frac{v_{\text{esc},j}}{v_{K,j}} = \left[\frac{2G(M_j + M_{j+1})}{R_j + R_{j+1}} \right]^{1/2} \left[\frac{GM_*}{(a_j + a_{j+1})/2} \right]^{-1/2} = h_j \left(6 \frac{r_{H,j}}{R_j + R_{j+1}} \right)^{1/2}. \quad (8)$$

Note that $r_{K,j}$ consists of the Hill radius $r_{H,j}$ and the Hill-to-physical radius ratio $r_{H,j}/(R_j + R_{j+1})$. This Hill-to-physical radius ratio $\propto a^{1/2}$ indicates the dependence of the relative importance of gravitational scattering against collisions on the semimajor axis. We calculate the orbital architecture parameters \tilde{b}_K and \tilde{e}_K normalized by $r_{K,j}$ in the same way as Eqs.(5) and (6), which are given in Table 2. In Figure 4, we plot \tilde{b}_K and \tilde{e}_K against $\langle a_M \rangle$ (models S0 and R1-3). We find that $\langle \tilde{b}_K \rangle$ and $\langle \tilde{e}_K \rangle$ are almost independent of $\langle a_M \rangle$ with weak dependencies of $d \log \langle \tilde{b}_K \rangle / d \log \langle a_M \rangle \simeq -0.1$ and $d \log \langle \tilde{e}_K \rangle / d \log \langle a_M \rangle \simeq 0.1$. This means that the a_M -dependence is renormalized in scaling with r_K , which shows that for the orbital architecture, r_K is a more general scaling unit than r_H . Note that this r_K scaling is reduced to the Hill scaling for the fixed Hill-to-physical radius ratio, as in section 3.2, which again shows \tilde{b}_K and \tilde{e}_K independent of M_{tot} (models S0 and M1-3) as in Table 2. In this new scaling, the orbital architecture is approximately given as $\langle \tilde{b}_K \rangle \simeq 2.2 \pm 0.3$ and $\langle \tilde{e}_K \rangle \simeq 0.3 \pm 0.1$. For an equal-mass system, r_K can be approximated by

$$r_K \simeq ka \simeq 0.011 \left(\frac{M}{M_{\oplus}} \right)^{1/3} \left(\frac{\rho}{3 \text{ g cm}^{-3}} \right)^{1/6} \left(\frac{a}{0.1 \text{ au}} \right)^{3/2} \left(\frac{M_*}{M_{\odot}} \right)^{-1/2} \text{ au}. \quad (9)$$

In summary, the above results clearly show that the basic orbital architecture of planetary systems formed by giant impacts is scaled by r_K , in other words, v_{esc} determines the spatial structure of planetary systems. The results of our N -body simulations, $\tilde{b}_K \simeq 2$, justify the assumptions in some planet accretion models (e.g., [Schlichting 2014](#); [Weiss et al. 2023](#)).

4. SUMMARY AND DISCUSSION

This study aims to obtain the fundamental scaling laws for the orbital architecture of planetary systems self-organized by gravitational scattering and collision among protoplanets. We have investigated the orbital architecture of planetary systems formed from protoplanet systems by giant impacts using N -body simulations. We systematically changed the mass and location of the initial protoplanet systems and investigated their effects on the final planetary systems. We found that the mean orbital separation and eccentricity of planetary systems normalized by the Hill radius are nearly independent of the total mass of the initial protoplanet systems, which means that the Hill radius scales the orbital

architecture. On the other hand, they show a positive dependence on the system semimajor axis. This dependence can be scaled by the eccentric distance for the eccentricity given by the ratio between the two-body surface escape velocity and the Keplerian circular velocity r_K . We showed that the orbital architecture of planetary systems formed by giant impacts is scaled by r_K , which consists of the Hill radius and the Hill-to-physical radius ratio. In other words, r_K is an appropriate gravitational and collisional dynamics metric. In units of r_K , the mean orbital separation and the epicycle amplitude of a planetary system are 2.2 ± 0.3 and 0.3 ± 0.1 , respectively.

This scaling generally agrees with the observations. In this model, the separation, eccentricity, and inclination of planetary orbits increase with their semimajor axis. The orbital separations at $\simeq 0.1$ au and 1 au are consistent with those of the close-in super-Earths and the solar system terrestrial planets, respectively. Furthermore, this model also generally agrees with the peas-in-a-pod pattern. The orbital separation and mass deviations increase with the semimajor axis. In other words, the system uniformity diminishes with increasing the semimajor axis. These results mean that the peas-in-a-pod pattern diminishes with increasing the semimajor axis.

This scaling could be applied to systems of protoplanets initially in resonant chains. This is because the initial resonant configuration breaks down when the giant impact phase begins. Note that this model is only valid for $k \lesssim 1$. For $k \gtrsim 1$, planet ejection may occur (e.g., [Matsumoto et al. 2020](#)), which can modify the scaling.

The present analysis with idealized models provides a context for further studies with more realistic models. In a subsequent paper, we will further explore the parameter dependence of the orbital architecture to confirm the universality of the scaling. We also plan to investigate the effects of initial resonant configurations and planet ejection on the orbital architecture.

E.K. is supported by JSPS KAKENHI Grants No. 18H05438, 24K00698 and 24H00017. R.S. is partially supported by ISF, MOS, and NSF/BSF, and GIF grants. Numerical computations were partially conducted on the PC cluster at the Center for Computational Astrophysics, National Astronomical Observatory of Japan. This research was supported in part by the Munich Institute for Astro-, Particle and BioPhysics (MIAPbP) funded by the Deutsche Forschungsgemeinschaft (DFG, German Research Foundation) under Germany’s Excellence Strategy – EXC-2094 – 390783311 and by grant NSF PHY-2309135 to the Kavli Institute for Theoretical Physics (KITP).

REFERENCES

- Baruteau, C., & Papaloizou, J. C. B. 2013, *ApJ*, 778, 7,
doi: [10.1088/0004-637X/778/1/7](#)
- Batalha, N. M., Rowe, J. F., Bryson, S. T., et al. 2013,
ApJS, 204, 24, doi: [10.1088/0067-0049/204/2/24](#)
- Chambers, J. E., & Wetherill, G. W. 1998, *Icarus*, 136, 304,
doi: [10.1006/icar.1998.6007](#)
- Ghosh, T., & Chatterjee, S. 2024, *MNRAS*, 527, 79,
doi: [10.1093/mnras/stad2962](#)
- Goldberg, M., & Batygin, K. 2022, *AJ*, 163, 201,
doi: [10.3847/1538-3881/ac5961](#)
- Hadden, S., & Lithwick, Y. 2017, *AJ*, 154, 5,
doi: [10.3847/1538-3881/aa71ef](#)
- Hansen, B. M. S., & Murray, N. 2012, *ApJ*, 751, 158,
doi: [10.1088/0004-637X/751/2/158](#)
- He, M. Y., Ford, E. B., Ragozzine, D., & Carrera, D. 2020,
AJ, 160, 276, doi: [10.3847/1538-3881/abba18](#)
- Hoshino, H., & Kokubo, E. 2023, *MNRAS*, 519, 2838,
doi: [10.1093/mnras/stac3756](#)
- Howard, A. W., Marcy, G. W., Bryson, S. T., et al. 2012,
ApJS, 201, 15, doi: [10.1088/0067-0049/201/2/15](#)
- Kokubo, E., & Genda, H. 2010, *ApJL*, 714, L21,
doi: [10.1088/2041-8205/714/1/L21](#)
- Kokubo, E., & Ida, S. 1996, *Icarus*, 123, 180,
doi: [10.1006/icar.1996.0148](#)
- . 1998, *Icarus*, 131, 171, doi: [10.1006/icar.1997.5840](#)
- . 2002, *ApJ*, 581, 666, doi: [10.1086/344105](#)
- . 2012, *Progress of Theoretical and Experimental Physics*, 2012, 01A308, doi: [10.1093/ptep/pts032](#)
- Kokubo, E., Kominami, J., & Ida, S. 2006, *ApJ*, 642, 1131,
doi: [10.1086/501448](#)
- Kokubo, E., & Makino, J. 2004, *PASJ*, 56, 861,
doi: [10.1093/pasj/56.5.861](#)

- Kokubo, E., Yoshinaga, K., & Makino, J. 1998, MNRAS, 297, 1067, doi: [10.1046/j.1365-8711.1998.01581.x](https://doi.org/10.1046/j.1365-8711.1998.01581.x)
- Lee, E. J., & Chiang, E. 2016, ApJ, 817, 90, doi: [10.3847/0004-637X/817/2/90](https://doi.org/10.3847/0004-637X/817/2/90)
- Lissauer, J. J., Dawson, R. I., & Tremaine, S. 2014, Nature, 513, 336, doi: [10.1038/nature13781](https://doi.org/10.1038/nature13781)
- Makino, J. 1991, PASJ, 43, 859
- Matsumoto, Y., Gu, P.-G., Kokubo, E., Oshino, S., & Omiya, M. 2020, A&A, 642, A23, doi: [10.1051/0004-6361/202038332](https://doi.org/10.1051/0004-6361/202038332)
- Matsumoto, Y., & Kokubo, E. 2017, AJ, 154, 27, doi: [10.3847/1538-3881/aa74c7](https://doi.org/10.3847/1538-3881/aa74c7)
- Mayor, M., Marmier, M., Lovis, C., et al. 2011, arXiv e-prints, arXiv:1109.2497, doi: [10.48550/arXiv.1109.2497](https://doi.org/10.48550/arXiv.1109.2497)
- Millholland, S. C., & Winn, J. N. 2021, ApJL, 920, L34, doi: [10.3847/2041-8213/ac2c77](https://doi.org/10.3847/2041-8213/ac2c77)
- Nitadori, K., Makino, J., & Hut, P. 2006, NewA, 12, 169, doi: [10.1016/j.newast.2006.07.007](https://doi.org/10.1016/j.newast.2006.07.007)
- Ogihara, M., Kokubo, E., Suzuki, T. K., & Morbidelli, A. 2018, A&A, 615, A63, doi: [10.1051/0004-6361/201832720](https://doi.org/10.1051/0004-6361/201832720)
- Petigura, E. A., Howard, A. W., Marcy, G. W., et al. 2017, AJ, 154, 107, doi: [10.3847/1538-3881/aa80de](https://doi.org/10.3847/1538-3881/aa80de)
- Raymond, S. N., Kokubo, E., Morbidelli, A., Morishima, R., & Walsh, K. J. 2014, in Protostars and Planets VI, ed. H. Beuther, R. S. Klessen, C. P. Dullemond, & T. Henning, 595–618, doi: [10.2458/azu_uapress_9780816531240-ch026](https://doi.org/10.2458/azu_uapress_9780816531240-ch026)
- Safronov, V. S. 1972, Evolution of the protoplanetary cloud and formation of the earth and planets.
- Schlichting, H. E. 2014, ApJL, 795, L15, doi: [10.1088/2041-8205/795/1/L15](https://doi.org/10.1088/2041-8205/795/1/L15)
- Weiss, L. M., Millholland, S. C., Petigura, E. A., et al. 2023, in Astronomical Society of the Pacific Conference Series, Vol. 534, Protostars and Planets VII, ed. S. Inutsuka, Y. Aikawa, T. Muto, K. Tomida, & M. Tamura, 863
- Weiss, L. M., Marcy, G. W., Petigura, E. A., et al. 2018, AJ, 155, 48, doi: [10.3847/1538-3881/aa9ff6](https://doi.org/10.3847/1538-3881/aa9ff6)
- Winn, J. N., & Fabrycky, D. C. 2015, ARA&A, 53, 409, doi: [10.1146/annurev-astro-082214-122246](https://doi.org/10.1146/annurev-astro-082214-122246)
- Xie, J.-W., Dong, S., Zhu, Z., et al. 2016, Proceedings of the National Academy of Science, 113, 11431, doi: [10.1073/pnas.1604692113](https://doi.org/10.1073/pnas.1604692113)
- Zhu, W., Petrovich, C., Wu, Y., Dong, S., & Xie, J. 2018, ApJ, 860, 101, doi: [10.3847/1538-4357/aac6d5](https://doi.org/10.3847/1538-4357/aac6d5)